Application of the RBF collocation method to transient coupled thermoelasticity

Boštjan Mavrič

Institute of Metals and Technology, Ljubljana, Slovenia, and

Božidar Šarler

*Faculty of Mechanical Engineering, University of Ljubljana, Ljubljana, Slovenia
and Institute of Metals and Technology, Ljubljana, Slovenia*

Abstract

Purpose – In this study, the authors aim to upgrade their previous developments of the local radial basis function collocation method (LRBFCM) for heat transfer, fluid flow, electromagnetic problems and linear thermoelasticity to dynamic-coupled thermoelasticity problems.

Design/methodology/approach – The authors solve a thermoelastic benchmark by considering a linear thermoelastic plate under thermal and pressure shock. Spatial discretization is performed by a local collocation with multi-quadrics augmented by monomials. The implicit Euler formula is used to perform the time stepping. The system of equations obtained from the formula is solved using a Newton–Raphson algorithm with GMRES to iteratively obtain the solution. The LRBFCM solution is compared with the reference finite-element method (FEM) solution and, in one case, with a solution obtained using the meshless local Petrov–Galerkin method.

Findings – The performance of the LRBFCM is found to be comparable to the FEM, with some differences near the tip of the shock front. The LRBFCM appears to converge to the mesh-converged solution more smoothly than the FEM. Also, the LRBFCM seems to perform better than the MLPG in the studied case.

Research limitations/implications – The performance of the LRBFCM near the tip of the shock front appears to be suboptimal because it does not capture the shock front as well as the FEM. With the exception of a solution obtained using the meshless local Petrov–Galerkin method, there is no other high-quality reference solution for the considered problem in the literature yet. In most cases, therefore, the authors are able to compare only two mesh-converged solutions obtained by the authors using two different discretization methods. The shock-capturing capabilities of the method should be studied in more detail.

Originality/value – For the first time, the LRBFCM has been applied to problems of coupled thermoelasticity.

Keywords Local radial basis function collocation method, Meshless methods, Multi-quadrics, Coupled thermoelasticity

Paper type Research paper

1. Introduction

Thermomechanical phenomena are important in many different fields of science and engineering, because they have a significant impact on constructions and parts that either

www.

undergo repeated loading or reheating cycles or are exposed to rapid changes in the load or temperature. The stresses generated during these kinds of events greatly affect the reliability and failure rate of engineering parts and scientific equipment. Therefore, a considerable effort is made to develop new methods to model this kind of phenomenon.

To accurately model coupled thermoelasticity problems, we need to simultaneously solve two sets of equations:

(1) a hyperbolic equation of motion for elastic deformation; and

(2) a parabolic equation governing the heat conduction.

The different natures of the governing equations prevent us from obtaining any analytical solutions for the fully coupled problem. The exact solutions can only be obtained if we omit the full coupling, as was the case in the fundamental work of Danilovskaya (1952) and Boley and Tolins (1962). To verify the numerical methods on fully coupled problems, we are limited to cross-code comparisons.

Because numerical methods are of great practical importance in the field of coupled thermomechanics, many reference solutions using different approaches can be found from traditional methods used in commercial codes, to contemporary methods including a large spectrum of meshless approaches (Gao *et al.*, 2015; Hosseini-Tehrani and Eslami, 2000; Sladek *et al.*, 2009, 2006).

In this paper, the local radial basis function collocation method (LRBFCM) is extended to coupled thermoelasticity problems. The method uses a strong formulation. It calculates the discretized differential operators using a local interpolant constructed from radial basis functions and linear monomials. The LRBFCM was first introduced to solve heat-diffusion problems by Šarler and Vertnik (2006). The method has been successfully applied to many different fields in science and engineering (Kosec and Šarler, 2014; Mramor *et al.*, 2013; Vertnik and Šarler, 2011), including the work done by the present authors in the field of solid mechanics (Mavrič and Šarler, 2015a, 2015b).

In this paper, we first present the governing equations and boundary conditions of the posed problem (Hosseini-Tehrani and Eslami, 2000). The solution procedure based on the LRBFCM is presented subsequently. The formulation of the method is followed by a short discussion of the implementation details followed by the result for the following three cases: the temperature-driven shock, the pressure-driven shock and the combination of both.

The results are compared with a reference solution calculated using the finite-element method (FEM) implemented in FreeFem++ (Hecht, 2012) and, for the case of thermal shock, with the solution presented in (Zheng *et al.*, 2015) obtained by using a novel meshless local Petrov–Galerkin method.

2. Governing equations
In this paper, we consider the problem of coupled thermoelasticity (Fung and Tong, 2008) given by the following system of equations:

$$\rho c_p \dot{T} = k\nabla^2 T - \beta T_0 \nabla \cdot \boldsymbol{v}$$
$$\rho \dot{\boldsymbol{v}} = (\lambda + 2G)\nabla^2 \boldsymbol{u} + (\lambda + G)\nabla(\nabla \cdot \boldsymbol{u}) - \beta \nabla(T - T_0) \qquad (1)$$
$$\dot{\boldsymbol{u}} = \boldsymbol{v}$$

The equations couple the temperature T, the deformation $\boldsymbol{u}$ and the deformation rate $\boldsymbol{v}$. The material is described by its density ρ, heat capacity c_p, thermal conductivity k and the thermoelastic coupling parameter $\beta = (\lambda + 2G)\alpha$, where α is the thermal expansion parameter.

The material's mechanical properties are given by the Lamé parameters λ and G. The reference temperature at which the thermal strains are assumed to be zero is denoted by T_0.

The system of governing equations can be given in terms of dimensionless variables (Hosseini-Tehrani and Eslami, 2000):

$$\dot{\hat{T}} = \nabla^2 \hat{T} - \frac{T_0 \beta^2}{\rho c_p (\lambda + 2G)} \nabla \cdot \hat{\boldsymbol{v}}$$

$$\dot{\hat{\boldsymbol{v}}} = \frac{g}{\lambda + 2G} \nabla^2 \hat{\boldsymbol{u}} \frac{\lambda + G}{\lambda + 2G} \nabla (\nabla \cdot \hat{\boldsymbol{u}}) - \nabla \hat{T}. \tag{2}$$

The dimensionless quantities are more appropriate when we want to compare different solutions. The dimensionless variables are defined as follows:

$$\hat{x} = \frac{x}{l}, \hat{t} = \frac{tc}{l}, \hat{\sigma} = \frac{\sigma}{\beta T_0}, \hat{T} = \frac{T - T_0}{T_0}, \hat{\boldsymbol{u}} = \frac{\lambda + G}{\beta} \boldsymbol{u}. \tag{3}$$

We use them to state our results in the rest of the paper, with the hats omitted for convenience. In the definition of the dimensionless variables in equations (3), $l = k/\rho c_p c$ is the characteristic length and $c = \sqrt{\lambda + 2G/\rho}$ is the speed of the longitudinal waves.

In our code, the system of equations (1) is implemented in dimensional form. The calculation in dimensionless variables is performed by selecting the material properties, as specified in Table I. To state the results in terms of dimensionless variables uniquely, the Poisson ratio also needs to be known. In this investigation, the value $\nu = 0.3$ is used.

The introduction of dimensionless variables also adds an additional dimensionless parameter, called the thermoelastic parameter C, given by:

$$C = \frac{T_0 \beta^2}{\rho C (\lambda + 2G)} \tag{4}$$

The thermoelastic parameter gives us the amplitude of the coupling between the deformation and the temperature field. The case of uncoupled thermoelasticity is obtained by setting $C = 0$, meaning that the thermal transport is independent of the deformation, which is the assumption made in most practical studies.

2.1 Boundary conditions
The benchmark case is the same as the one considered by Hosseini-Tehrani and Eslami (2000) and, with some minor modifications, by Zheng et al. (2015). We are considering a

Material property	Value
ρ	1 kg/m^3
c_p	1 J/kg
k	$1 \text{ W/m}^2\text{K}$
E	$3 + 2\nu + 2/(\nu - 1)$
ν	0.3
α	$(1 - 2\nu)/E$

Table I.
Values of the material properties used to perform the calculations in dimensionless variables

www.

square domain with a side length 10, as illustrated in Figure 1. The domain is thermally isolated on all sides $\mathbf{n} \cdot \nabla T = 0$, except for the side at $x_1 = 0$, where the temperature is specified. The top ($x_2 = 10$) and bottom ($x_2 = 0$) of the domain are traction free, whereas the deformation at side $x_1 = 10$ is set to zero. On the side $x_1 = 0$, the traction in the x_1 direction is specified as required for different benchmark cases.

3. Solution procedure
3.1 Domain discretization and subdomain selection
The problem is considered in the domain Ω with the boundary Γ. A node-generation method is used to position the nodes, both in the domain and on the boundary. In our case, we use a simple regular grid, but a more general positioning can easily be used. We select a certain number ($_lN$) of nearby nodes as the influence domain for each node l in the computational domain, which results in the local nature of the method. In the present paper, we use the nearest neighbors as a way of determining the domains of influence. The choice of subdomains induces a mapping $_ls: i \rightarrow k$ from the local index i of the subdomain l, ranging from 1 to $_lN$, to the global index k that is assigned to each of the nodes.

3.2 Construction of local interpolants
On each influence domain, the solution is locally interpolated with an RBF interpolant. In our case, we use rescaled multi-quadrics, which are known to provide a very good interpolation accuracy (Larsson and Fornberg, 2005) and were already studied for thermoelastic problems in Mavrič and Šarler (2015b). In the latter, the convergence was analyzed with respect to the number of local collocation points $_lN$, the selection of augmentation monomials and the value of the RBF shape parameter. The multiquadrics are given by:

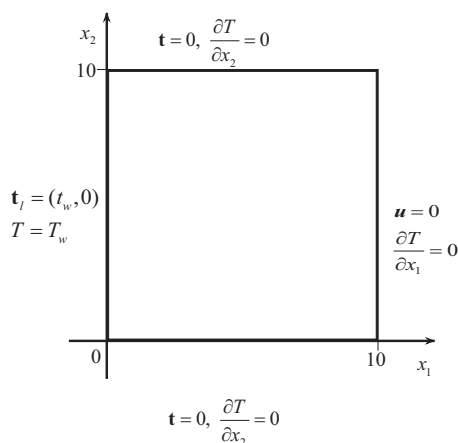$$\Phi_l(\mathbf{r}) = \sqrt{\left(\frac{\epsilon}{_lh_0}\right)^2 |\mathbf{r} - \mathbf{r}_l|^2 + 1}. \tag{5}$$

Figure 1.
Illustration of the boundary conditions

Here, ϵ is the dimensionless shape parameter, $_lh_0$ is the appropriate scaling factor and $\mathbf{r}_l$ is the position of l-th node, on which the multiquadric is centered. The scaling factor $_lh_0$ causes our approximation to be stationary (Wendland, 2004) and the shape parameter ϵ to be dimensionless. The scaling parameter describing the spatial scale of the influence domain is calculated using:

$$_lh_0 = \sqrt{\frac{\sum_{i=1}^{lN} |\mathbf{r}_{ls(i)} - \mathbf{r}_l|^2}{_lN - 1}} \tag{6}$$

Once the subdomain has been chosen for every node, the interpolant for each physical field present in the governing equations is constructed over each subdomain. The interpolant for the field $\boldsymbol{q}$, which can be a vector or a scalar field, in the l-th influence domain, is given by:

$$q_{\xi l}(\mathbf{r}) = \sum_{i=1}^{lN} {}_l\alpha_{i,\xi} \Phi_{ls(i)}(\mathbf{r}) + \sum_{i={}_lN+1}^{lN+aN} {}_l\alpha_{i,\xi} p_i(\mathbf{r} - \mathbf{r}_l) = \sum_{i=1}^{lN+aN} {}_l\alpha_{i,\xi} \Psi_i(\mathbf{r}), \xi = 1, 2. \tag{7}$$

The monomials $p_i(\mathbf{r})$ are used to augment the basis and contribute to a significant improvement of the method's performance in our setting (Mavrič and Šarler, 2015b). The number of augmentation monomials $_aN$ is set to three in this work, meaning that the constant and two linear functions (x_1-$x_{1, l}$, x_2-$x_{2, l}$) are added to the set of basis functions.

The constructed interpolant can then be used to calculate any linear differential operator D acting on the physical field $\boldsymbol{q}(\mathbf{r})$. Because the interpolation coefficients are constant over each influence domain we see that:

$$\mathcal{D}\boldsymbol{q}(\mathbf{r}) = \sum_{\chi} D_{\xi,\chi}(\mathbf{r}) q_{\chi}(\mathbf{r}) \approx \sum_{i,\chi}^{lN_aN} {}_l\alpha_{i,\chi} D_{\xi,\chi}(\mathbf{r}) \Psi_i(\mathbf{r}) \tag{8}$$

Because the action of the linear differential operator on the basis functions is known, the value of the differential operator is now restated in terms of the coefficients $_l\alpha_{i,\xi}$.

The unknown coefficients $_l\alpha_{i,\xi}$ are determined by writing out the interpolation equation of the field values at each point in the influence domain. If the point lies on the boundary, where the linear boundary condition $B_{\xi\chi}(\mathbf{r}) q_{\xi}(\mathbf{r}) = b_{\chi}(\mathbf{r})$. The system of equations for each subdomain l can be written in matrix form as:

$$\sum_{i,\zeta} {}_lA_{ji,\xi\zeta} {}_l\alpha_{i,\zeta} = {}_l\gamma_{j,\xi} \tag{9}$$

The right-hand-side vector γ and the matrix A are given by:

$$_lA_{ji,\xi\chi} = \begin{cases} \Psi_i(\mathbf{r}_{ls(j)}) \delta_{\xi\chi} & \text{if } \mathbf{r}_{ls(j)} \in \Omega \\ B_{\xi\chi}(\mathbf{r}_{ls(j)}) \Psi_i(\mathbf{r}_{ls(j)}) & \text{if } \mathbf{r}_{ls(j)} \in \Gamma \\ p_j(\mathbf{r}_{ls(i)}) & \text{if } j > {}_lN \wedge i < {}_lN \\ 0 & \text{otherwise} \end{cases}, \quad _l\gamma_{j,\xi} = \begin{cases} q_{\xi}(\mathbf{r}_{ls(j)}) & \text{if } \mathbf{r}_{ls(j)} \in \Omega \\ b_{\chi}(\mathbf{r}_{ls(j)}) & \text{if } \mathbf{r}_{ls(j)} \in \Gamma \\ 0 & \text{if } j > {}_lN \end{cases} \tag{10}$$

3.3 Application to differential operators

What remains to be completed in order to calculate the values of the differential operators is to combine equations (8) and (9). The unknown coefficients $_l\alpha_{i,\xi}$ are formally calculated by inverting the system of linear equation (9):

$$_l\alpha_{j,\xi} = \sum_{k,\zeta}^{lN+aN} {_lA_{jk,\xi\zeta}^{-1}} {_l\gamma_{k,\zeta}} \tag{11}$$

This results in the following expression for the value of the differential operator:

$$\mathcal{D}\boldsymbol{q}(\mathbf{r}) \approx \sum_{k,\chi}^{lN,aN} {_l\gamma_{k,\chi}} \sum_{i,\zeta}^{lN,aN} {_lA_{ik,\zeta\chi}^{-1}} D_{\xi\zeta}(\mathbf{r})\Psi_i(\mathbf{r}) \tag{12}$$

Recalling that the elements $_l\gamma_{k,\chi}$ contain either the values of the field in the nodes in the influence domain or the boundary conditions, we obtain an explicit expression for the value of the differential operator.

3.4 Time stepping

The LRBFCM only allows us to obtain expressions for discretized operators on the specific node arrangement. The variables are assembled in a column $\underline{Y} = [\boldsymbol{v}, \boldsymbol{u}, T]^T$ to perform the time stepping. The set of governing equations then becomes $\underline{\dot{Y}} = G(\underline{Y}, t)$. The implicit Euler method is used to perform the time stepping. The obtained system of equations is solved by using the Newton–Raphson method, using GMRES with an ILU0 preconditioner to solve the linearized system. The Jacobian is numerically calculated using forward difference formulas at each iteration step. The time stepping is performed using a constant time step of $\Delta t = 0.01$ for both spatial discretization approaches.

4. Numerical results

4.1 The reference FEM solution and mesh convergence

The free package FreeFem++ (Hecht, 2012) was used to calculate the reference FEM solution. The FEM discretization was performed by using Lagrange $\mathbb{P}_2$ elements on a triangulated square mesh. The discretization uses three times as many interior degrees of freedom, as there are discretization points. The domain discretizations for both approaches are shown in Figure 2.

The mesh convergence of the FEM solution is shown in Figure 3. The plot shows the axial deformation, the axial stress and the temperature for the case of a pressure shock with the thermomechanical parameter set to $C = 0.1$. All the quantities are displayed for two times, i.e. $t = 3$ and $t = 6$, for different values of the number of discretization points along one dimension N. We see that there is no significant difference between the solutions for $N = 25$ and $N = 50$, so we take the solution with $N = 50$ as the mesh-converged reference solution.

In the same manner, the LRBFCM mesh convergence is studied in Figure 4. We use nine nodes per influence domain and the shape parameter value $\epsilon = 2\cdot10^{-4}$, which we find to be a good choice for the considered problem (Mavrič and Šarler, 2015b). Again, we notice that there is no significant difference between the solutions for $N = 75$ and $N = 151$, so we use the solution for $N = 151$ as the mesh-converged LRBFCM solution. It is also clear that the LRBFCM gives somewhat smoother results than the FEM for a given number of unknowns.

4.2 Thermal shock

A thermal shock is applied to the plate by setting $T_w = 5t \exp(-2t)$ and $t_w = 0$. The results along the centerline at $x_2 = 5$ are shown for the times $t = 3$ and $t = 6$. In Figure 5, the axial deformation u_1 is shown, Figure 6 shows the axial stress σ_{11} and Figure 7 shows the temperature T. It is clear that the FEM and the LRBFCM solutions match well qualitatively.

Figure 2.
Illustration of the spatial structure used for the discretization: the triangular FEM mesh on the left and the LRBFCM node arrangement on the right
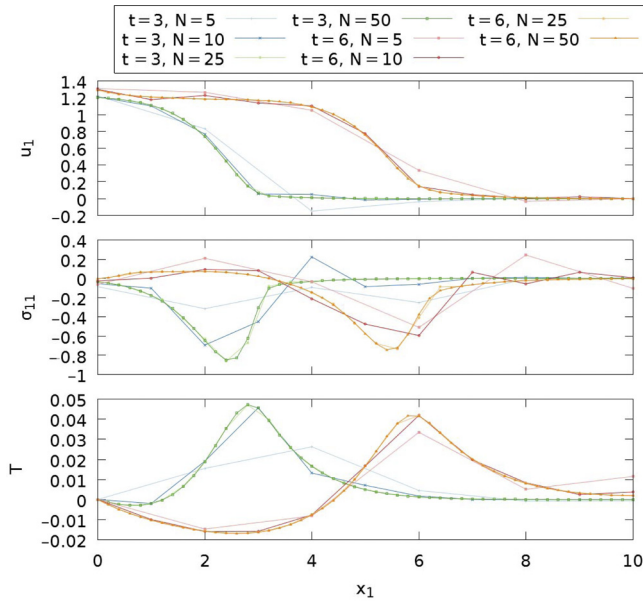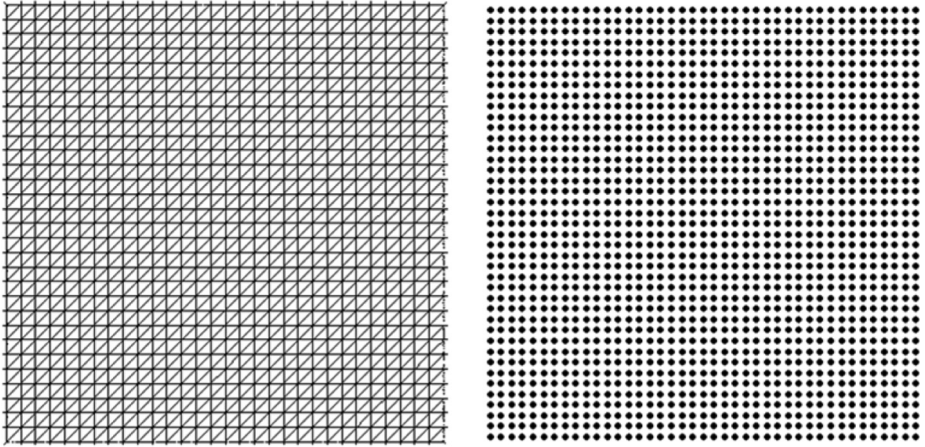
Figure 3.
Study of the mesh convergence of the reference FEM solution
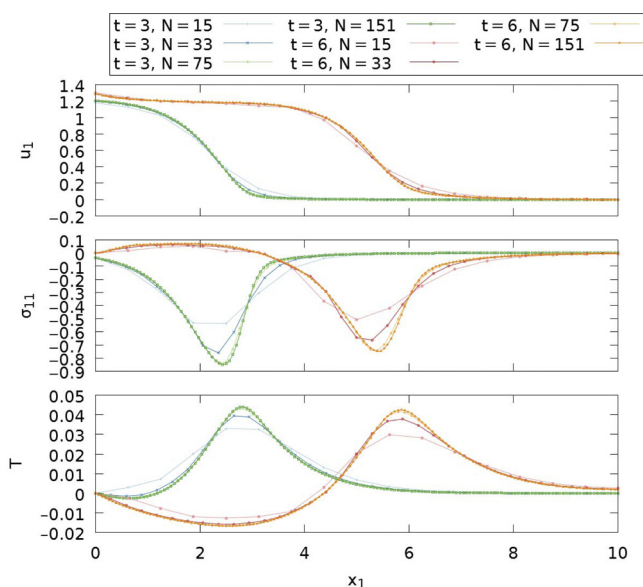
Notes: Results are shown for the case of pressure shock and the thermomechanical coupling parameter set to $C = 0.1$

Figure 4.
Study of the mesh
convergence of the
LRBFCM solution
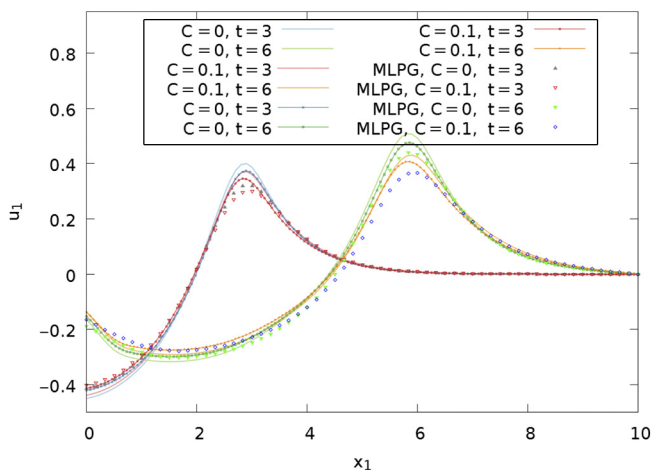
Notes: Results are shown for the case of pressure shock and the
thermomechanical coupling parameter set to $C = 0.1$
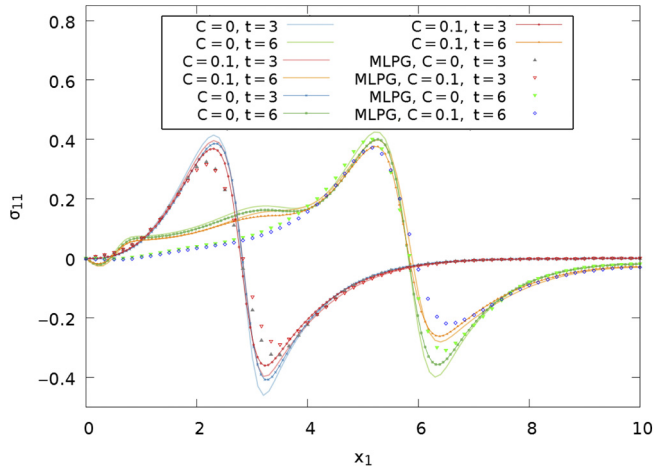

Figure 5.
Comparison of the
axial deformation for
thermal shock
loading

Notes: The FEM solution is shown with lines and the LRBFCM
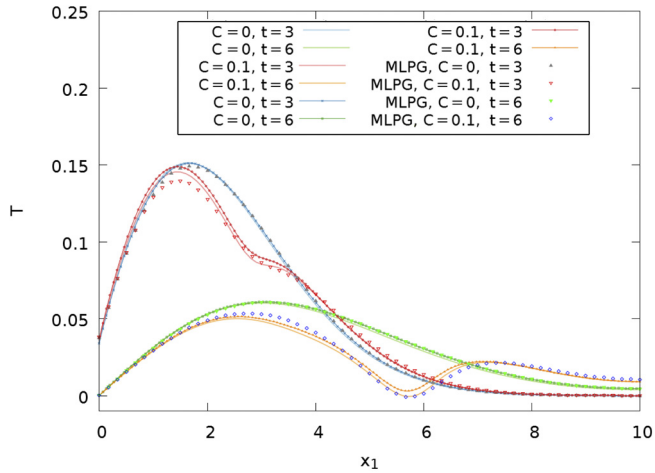solution using lines with points. The MLPG solution is shown
with points only

Figure 6.
Comparison of the
axial stress for
thermal shock
loading

Notes: The FEM solution is shown with lines and the LRBFCM
solution using lines with points. The MLPG solution is shown
with points only

Figure 7.
Comparison of the
temperature for
thermal shock
loading

Notes: The FEM solution is shown with lines and the LRBFCM
solution using lines with points. The MLPG solution is shown
with points only

The LRBFCM solution underestimates the peak values of the deformation and stress, but it
performs well when calculating the temperature field. By neglecting the areas around the
shock front, we can see that the LRBFCM matches well with the FEM solution, especially
good matching is observed for the case of the axial stress at $t = 6$ and $x_1 < 3$. In this area, the

information from the boundary conditions at $x_2 = 0$ and $x_2 = 10$ reaches the centerline. A good match in this area means that the LRBFCM correctly calculates the coupling between the two vector components of the solution.

In this case, we can also compare the results with those obtained using MLPG, published in a recent paper Zheng *et al.* (2015). We can see that the MLPG solution is even worse at calculating the peak values and does not reproduce the hump in the axial stress at $t = 6$ and $x_1 < 3$. The reason for this might be that the solution is not yet mesh-converged because the paper Zheng *et al.* (2015) claims to use a grid of only 13×13 nodes to discretize the governing equation. For this reason, we refrained from making any further comparisons with their results.

4.3 Pressure shock

The pressure shock is applied to the plate by setting $T_w = 0$ and $t_w = 5t \exp(-2t)$. We show the results in the same manner as for the previous case. In Figure 8, the axial deformation u_1 is shown, Figure 9 shows the axial stress σ_{11} and Figure 10 shows the temperature T. In this case, we see excellent agreement between the FEM and the LRBFCM solutions for both stress and deformation. Some differences are only present when comparing the temperature at $t = 3$, where the LRBFCM results are consistently higher than the FEM results.

4.4 Thermal and pressure shock in combination

Both shocks are applied to the plate in combination by setting $T_w = 5t \exp(-2t)$ and $t_w = 5t \exp(-2t)$. The results are shown in the same manner as for the previous case. In Figure 11, the axial deformation u_1 is shown, Figure 12 shows the axial stress σ_{11} and Figure 13 shows the temperature T.

Because the system of governing equations is linear, the solution to this problem is nothing but the sum of the two previous solutions and so are the differences between the FEM and the LRBFCM solutions. We can see good agreement between the solutions for the deformations
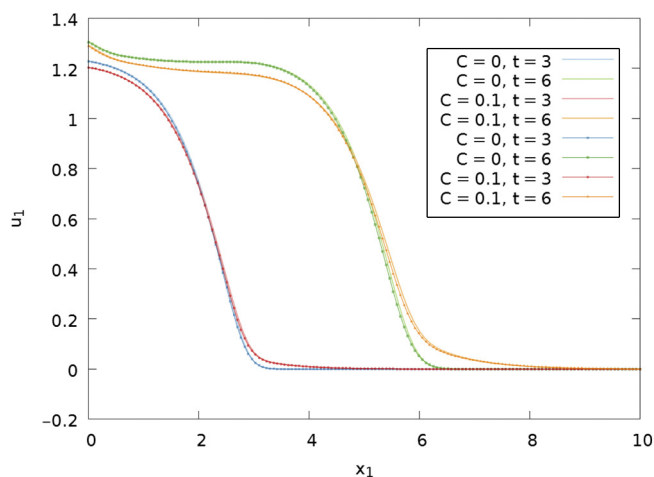
Notes: The FEM solution is shown with lines and the LRBFCM solution using lines with points
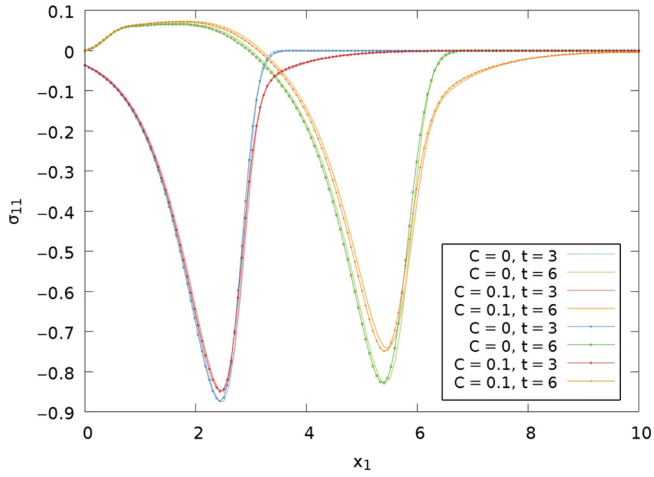
Notes: The FEM solution is shown with lines and the LRBFCM
solution using lines with points
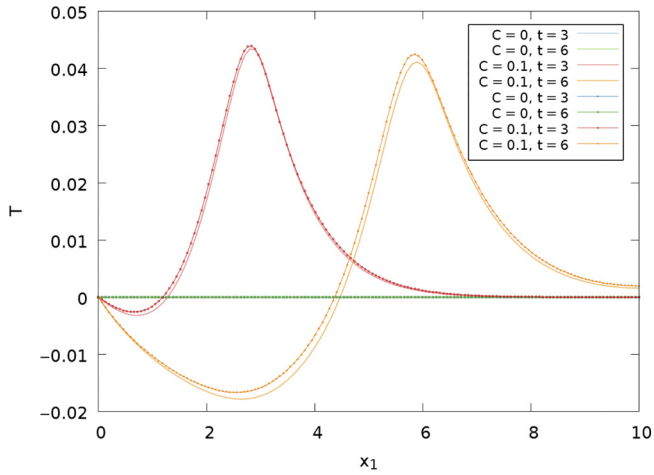
Notes: The FEM solution is shown with lines and the LRBFCM
solution using lines with points

and the stress. Larger differences can be seen when comparing the temperatures, where the
LRBFCM solution is again consistently higher than the FEM solution.

5. Conclusions

In this paper, we have demonstrated that the LRBFCM can compete with the FEM when
modelling coupled thermoelasticity. The LRBFCM solution matches well with the FEM
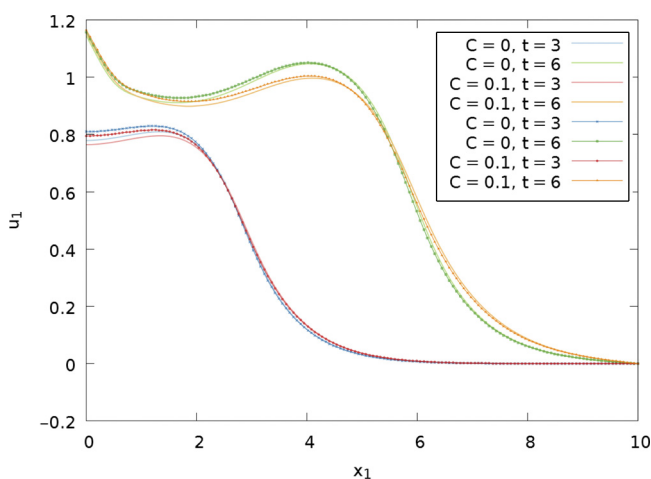
Notes: The FEM solution is shown with lines and the LRBFCM
solution using lines with points

Figure 11.
Comparison of the
deformation for the
simultaneous
application of thermal
and pressure shock
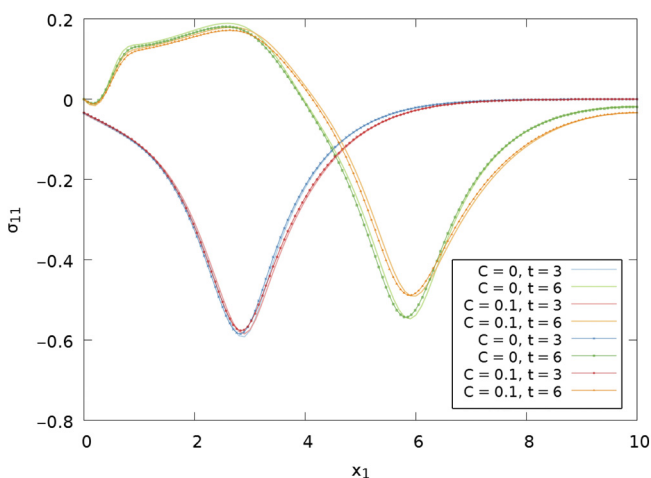
Notes: The FEM solution is shown with lines and the LRBFCM
solution using lines with points

Figure 12.
Comparison of the
axial stress for the
simultaneous
application of thermal
and pressure shock

solution, both qualitatively and quantitatively. Some differences remain in the ability to capture the shock front, where the FEM method performs slightly better; however, the LRBFCM method might be improved in this regard, as demonstrated in recent work done on shock-capturing using radial basis functions (Harris *et al.*, 2015).

The results presented in this paper differ significantly from the results shown in Zheng *et al.* (2015), although Zheng *et al.* find a good match between the MLPG and their reference
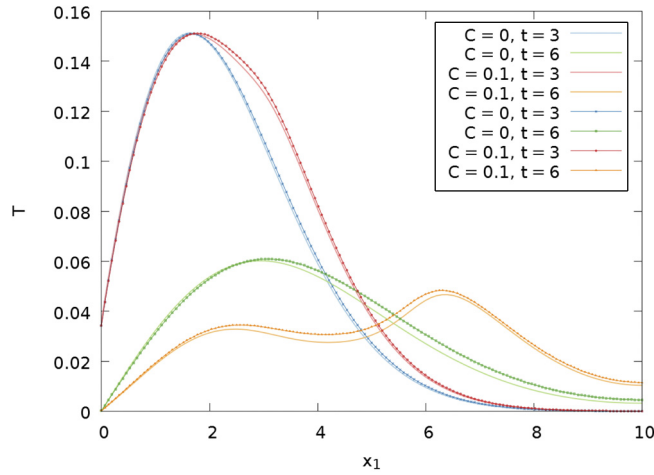
Notes: The FEM solution is shown with lines and the LRBFCM
solution using lines with points

FEM solution. We suspect that the reason for this is the small node count used when
calculating their results. They used a regular square grid consisting of only 13 nodes in each
direction. In contrast, we needed at least ten times as many discretization points in each
direction to obtain a mesh-converged solution. Also, their solution does not implement the
boundary conditions for the temperature in the case of the pressure-shock loading in the
same way as the pioneering reference solution obtained by Hosseini-Tehrani and Eslami
(2000) and, thus, further reduces the possibility of a cross-code comparison.

This work also validates the time-stepping procedure used, which we plan to use as a
core for further extensions of the LRBFCM to the rate-dependent viscoplasticity. The
iterative GMRES algorithm used in the inner loop also keeps the total computational time
linear with respect to the number of discretization points and thus is not prohibitively long
for large node counts.

References

Boley, B.A. and Tolins, I.S. (1962), "Transient coupled thermoelastic boundary value problems in the
half-space", *Journal of Applied Mechanics*, Vol. 29, pp. 637-646, doi: 10.1115/1.3640647.

Danilovskaya, V.I. (1952), "On a dynamical problem of thermoelasticity", *Prikl Mat Mekh*, Vol. 16,
pp. 341-344.

Fung, Y.C. and Tong, P. (2008), *Classical and Computational Solid Mechanics, Advanced Series in
Engineering Science*, World Scientific, Singapore.

Gao, X.-W., Zheng, B.-J., Yang, K. and Zhang, C. (2015), "Radial integration BEM for dynamic coupled
thermoelastic analysis under thermal shock loading", *Computers & Structures*, Vol. 158,
pp. 140-147, doi: 10.1016/j.compstruc.2015.06.006.

Harris, M., Kassab, A. and Divo, E. (2015), "Application of an RBF blending interpolation method to
problems with shocks", in Novak, A.J., Banaszek, J. and Šarler, B. (Eds), Conference Proceedings
Presented at the Numerical Heat Transfer 2015, Warsaw, p. 33.

Hecht, F. (2012), "New development in freefem++", *Journal of Numerical Mathematics*, Vol. 20, doi: 10.1515/jnum-2012-0013.

Hosseini-Tehrani, P. and Eslami, M.R. (2000), "BEM analysis of thermal and mechanical shock in a two-dimensional finite domain considering coupled thermoelasticity", *Engineering Analysis with Boundary Elements*, Vol. 24, pp. 249-257.

Kosec, G. and Šarler, B. (2014), "Simulation of macrosegregation with mesosegregates in binary metallic casts by a meshless method", *Engineering Analysis with Boundary Elements*, Vol. 45, pp. 36-44, doi: 10.1016/j.enganabound.2014.01.016.

Larsson, E. and Fornberg, B. (2005), "Theoretical and computational aspects of multivariate interpolation with increasingly flat radial basis functions", *Computers & Mathematics with Applications*, Vol. 49 No. 1, pp. 103-130.

Mavrič, B. and Šarler, B. (2015a), "Modelling of stress fields during LFEM DC casting of aluminium billets by a meshless method", *IOP Conference Series: Materials Science and Engineering*, Vol. 84 No. 1, p. 012099, doi: 10.1088/1757-899X/84/1/012099.

Mavrič, B. and Šarler, B. (2015b), "Local radial basis function collocation method for linear thermoelasticity in two dimensions", *International Journal of Numerical Methods for Heat & Fluid Flow*, Vol. 25 No. 6, pp. 1488-1510, doi: 10.1108/HFF-11-2014-0359.

Mramor, K., Vertnik, R. and Šarler, B. (2013), "Simulation of natural convection influenced by magnetic field with explicit local radial basis function collocation method", *Computer Modeling in Engineering and Sciences*, Vol. 92 No. 4, pp. 327-352.

Šarler, B. and Vertnik, R. (2006), "Meshfree explicit local radial basis function collocation method for diffusion problems", *Computers & Mathematics with Applications*, Vol. 51, pp. 1269-1282, doi: 10.1016/j.camwa.2006.04.013.

Sladek, J., Sladek, V., Solek, P., Tan, C.L. and Zhang, C. (2009), "Two-and three-dimensional transient thermoelastic analysis by the MLPG method", *Computer Modeling in Engineering and Sciences*, Vol. 47, pp. 61-95.

Sladek, J., Sladek, V., Zhang, C. and Tan, C.L. (2006), "Meshless local petrov-galerkin method for linear coupled thermoelastic analysis", *Computer Modeling in Engineering and Sciences*, Vol. 16, pp. 57-68.

Vertnik, R. and Šarler, B. (2011), "Local collocation approach for solving turbulent combined forced and natural convection problems", *Advances in Applied Mathematics and Mechanics*, Vol. 3 No. 3, pp. 259-279.

Wendland, H. (2004), *Scattered Data Approximation, Cambridge Monographs on Applied and Computational Mathematics*, Cambridge University Press.

Zheng, B.-J., Gao, X.-W. and Yang, K.C.-Z.Z. (2015), "A novel meshless local petrov–galerkin method for dynamic coupled thermoelasticity analysis under thermal and mechanical shock loading", *Engineering Analysis with Boundary Elements*, Vol. 60, pp. 154-161, doi: 10.1016/j.enganabound.2014.12.001.

Corresponding author
Božidar Šarler can be contacted at: bozidar.sarler@imt.si